Monthly Notices
of the
ROYAL ASTRONOMICAL SOCIETY

Mon. Not. R. Astron. Soc. **413,** 1777–1786 (2011) doi:10.1111/j.1365-2966.2011.18253.x

HerMES: SPIRE emission from radio-selected active galactic nuclei★

N. Seymour,[1]† M. Symeonidis,[1] M. J. Page,[1] A. Amblard,[2] V. Arumugam,[3] H. Aussel,[4] A. Blain,[5] J. Bock,[5,6] A. Boselli,[7] V. Buat,[7] N. Castro-Rodríguez,[8,9] A. Cava,[8,9] P. Chanial,[4] D. L. Clements,[10] A. Conley,[11] L. Conversi,[12] A. Cooray,[2,5] C. D. Dowell,[5,6] E. Dwek,[13] S. Eales,[14] D. Elbaz,[4] A. Franceschini,[15] J. Glenn,[11] E. A. González Solares,[16] M. Griffin,[14] E. Hatziminaoglou,[17] E. Ibar,[18] K. Isaak,[14] R. J. Ivison,[18,3] G. Lagache,[19] L. Levenson,[5,6] N. Lu,[5,20] S. Madden,[4] B. Maffei,[21] G. Mainetti,[15] L. Marchetti,[15] H. T. Nguyen,[5,6] B. O'Halloran,[10] S. J. Oliver,[22] A. Omont,[23] P. Panuzzo,[4] A. Papageorgiou,[14] C. P. Pearson,[24,25] I. Pérez-Fournon,[8,9] M. Pohlen,[14] J. I. Rawlings,[1] D. Rizzo,[10] I. G. Roseboom,[22] M. Rowan-Robinson,[10] B. Schulz,[5,20] Douglas Scott,[26] D. L. Shupe,[5,20] A. J. Smith,[22] J. A. Stevens,[27] M. Trichas,[28] K. E. Tugwell,[1] M. Vaccari,[15] I. Valtchanov,[12] L. Vigroux,[23] L. Wang,[22] G. Wright,[18] C. K. Xu[5,20] and M. Zemcov[5,6]

[1]*Mullard Space Science Laboratory, University College London, Holmbury St Mary, Dorking, Surrey RH5 6NT*
[2]*Department of Physics and Astronomy, University of California, Irvine, CA 92697, USA*
[3]*Institute for Astronomy, University of Edinburgh, Royal Observatory, Blackford Hill, Edinburgh EH9 3HJ*
[4]*Laboratoire AIM-Paris-Saclay, CEA/DSM/Irfu – CNRS – Université Paris Diderot, CE-Saclay, pt courrier 131, F-91191 Gif-sur-Yvette, France*
[5]*California Institute of Technology, 1200 E. California Blvd., Pasadena, CA 91125, USA*
[6]*Jet Propulsion Laboratory, 4800 Oak Grove Drive, Pasadena, CA 91109, USA*
[7]*Laboratoire d'Astrophysique de Marseille, OAMP, Université Aix-marseille, CNRS, 38 rue Frédéric Joliot-Curie, 13388 Marseille Cedex 13, France*
[8]*Instituto de Astrofísica de Canarias (IAC), E-38200 La Laguna, Tenerife, Spain*
[9]*Departamento de Astrofísica, Universidad de La Laguna (ULL), E-38205 La Laguna, Tenerife, Spain*
[10]*Astrophysics Group, Imperial College London, Blackett Laboratory, Prince Consort Road, London SW7 2AZ*
[11]*Department of Astrophysical and Planetary Sciences, CASA 389-UCB, University of Colorado, Boulder, CO 80309, USA*
[12]*Herschel Science Centre, European Space Astronomy Centre, Villanueva de la Cañada, 28691 Madrid, Spain*
[13]*Observational Cosmology Lab, Code 665, NASA Goddard Space Flight Center, Greenbelt, MD 20771, USA*
[14]*Cardiff School of Physics and Astronomy, Cardiff University, Queens Buildings, The Parade, Cardiff CF24 3AA*
[15]*Dipartimento di Astronomia, Università di Padova, vicolo Osservatorio 3, 35122 Padova, Italy*
[16]*Institute of Astronomy, University of Cambridge, Madingley Road, Cambridge CB3 0HA*
[17]*ESO, Karl-Schwarzschild-Str. 2, 85748 Garching bei München, Germany*
[18]*UK Astronomy Technology Centre, Royal Observatory, Blackford Hill, Edinburgh EH9 3HJ*
[19]*Institut d'Astrophysique Spatiale (IAS), bâtiment 121, Université Paris-Sud 11 and CNRS (UMR 8617), 91405 Orsay, France*
[20]*Infrared Processing and Analysis Center, MS 100-22, California Institute of Technology, JPL, Pasadena, CA 91125, USA*
[21]*School of Physics and Astronomy, The University of Manchester, Alan Turing Building, Oxford Road, Manchester M13 9PL*
[22]*Astronomy Centre, Department of Physics and Astronomy, University of Sussex, Brighton BN1 9QH*
[23]*Institut d'Astrophysique de Paris, UMR 7095, CNRS, UPMC Univ. Paris 06, 98 bis boulevard Arago, F-75014 Paris, France*
[24]*Space Science & Technology Department, Rutherford Appleton Laboratory, Chilton, Didcot, Oxfordshire OX11 0QX*
[25]*Institute for Space Imaging Science, University of Lethbridge, Lethbridge, AB T1K 3M4, Canada*
[26]*Department of Physics & Astronomy, University of British Columbia, 6224 Agricultural Road, Vancouver, BC V6T 1Z1, Canada*
[27]*Centre for Astrophysics Research, University of Hertfordshire, College Lane, Hatfield, Hertfordshire AL10 9AB*
[28]*Harvard–Smithsonian Center for Astrophysics, 60 Garden Street, Cambridge, MA 02138, USA*

Accepted 2010 December 21. Received 2010 December 21; in original form 2010 September 24

★*Herschel* is an ESA space observatory with science instruments provided by European-led Principal Investigator consortia and with important participation from NASA.

†E-mail: nps@mssl.ucl.ac.uk

ABSTRACT

We examine the rest-frame far-infrared emission from powerful radio sources with 1.4-GHz luminosity densities of $25 \leq \log(L_{1.4}/\mathrm{W\,Hz^{-1}}) \leq 26.5$ in the extragalactic *Spitzer* First Look Survey field. We combine *Herschel*/SPIRE flux densities with *Spitzer*/Infrared Array Camera and Multiband Imaging Photometer for *Spitzer* infrared data to obtain total (8–1000 μm) infrared luminosities for these radio sources. We separate our sources into a moderate, $0.4 < z < 0.9$, and a high, $1.2 < z < 3.0$, redshift sub-sample and we use *Spitzer* observations of a $z < 0.1$ 3CRR sample as a local comparison. By comparison to numbers from the Square Kilometre Array (SKA) Simulated Skies, we find that our moderate-redshift sample is complete and our high-redshift sample is 14 per cent complete. We constrain the ranges of mean star formation rates (SFRs) to be 3.4–4.2, 18–41 and 80–581 $\mathrm{M_\odot\,yr^{-1}}$ for the local, moderate- and high-redshift samples, respectively. Hence, we observe an increase in the mean SFR with increasing redshift which we can parametrize as $\sim(1+z)^Q$, where $Q = 4.2 \pm 0.8$. However, we observe no trends of mean SFR with radio luminosity within the moderate- or high-redshift bins. We estimate that radio-loud active galactic nuclei (AGN) in the high-redshift sample contribute 0.1–0.5 per cent to the total SFR density at that epoch. Hence, if all luminous starbursts host radio-loud AGN we infer a radio-loud phase duty cycle of 0.001–0.005.

Key words: galaxies: active – infrared: galaxies – radio continuum: galaxies.

1 INTRODUCTION

There is now strong evidence that powerful active galactic nuclei (AGN) played a key role in the evolution of galaxies. The correlation of central black hole and stellar bulge mass (Magorrian et al. 1998), and the increased prevalence of star formation (Giavalisco et al. 2004; Hopkins & Beacom 2006) and AGN activity (Wall et al. 2005; Aird et al. 2010) at earlier epochs suggest that the growth of the black hole is somehow related to the growth of the host galaxy. In the local Universe, we see little evidence of high star formation rates (SFRs) in galaxies with powerful radio-loud AGN activity (e.g. Condon et al. 1998; Mauch & Sadler 2007). In the distant Universe, $z > 1$, luminous radio galaxies (Seymour et al. 2007) and powerful starbursts (Borys et al. 2005; Casey et al. 2009) are both hosted by massive galaxies, suggesting a common parent population. The idea that these processes are likely to be connected at the epoch when black holes and galaxies went through their most rapid phases of growth has been invoked within various semi-analytical models in order to reconcile these models with observations (e.g. Springel et al. 2005).

This connection between central black hole growth and SFR is often considered in the context of 'feedback' process(es), as the former is postulated to regulate the latter. In particular there is observational evidence, as well as theoretical models, in which the jet from an AGN can produce either positive or negative feedback, where the jet, traced by its radio emission, stimulates or quenches star formation, respectively. There is some observational evidence of *positive* feedback, whereby star formation is triggered by an AGN jet, for example in Minkowski's Object by a jet from NGC 541 (van Breugel et al. 1985; Croft et al. 2006), as well as theoretical models which suggest that the shocks generated by jet propagation can trigger collapse of overdense clouds and lead to star formation (Fragile et al. 2004; Saxton et al. 2005). *Negative* feedback by AGN jets would likely require the removal of fuel for star formation, evidence for which are the powerful AGN-induced outflows which have been seen in high-redshift radio galaxies (Nesvadba et al. 2006, 2008). Such a scenario has also been proposed to regulate the growth of massive galaxies in semi-empirical models (Bower et al. 2006; Croton et al. 2006), but this process is only important globally at late times, $z < 1$. At earlier times, it would be most important in halting the growth of the most massive galaxies.

Star formation in powerful AGN has been difficult to trace so far. This difficulty is due to heavy contamination in traditional diagnostics by emission from the AGN (e.g. UV luminosity or optical emission-line strengths) as well as obscuration by gas and dust. However, the far-infrared (far-IR) presents a window in the electromagnetic spectrum where AGN emission is weak and star formation, if present, can dominate. AGN dust emission tends to peak in the near-IR/mid-IR, so far-IR emission should be a cleaner measure of SFR than other traditional methods. It is also possible to use the near-IR/mid-IR to model and subtract any potential AGN contribution to the far-IR (e.g. Hatziminaoglou et al. 2008).

There is evidence for extreme SFRs in many powerful high-redshift radio galaxies ($z > 2$, 1.4-GHz luminosity densities, $L_{1.4} \geq 10^{27}\,\mathrm{W\,Hz^{-1}}$; Miley & De Breuck 2008) from their strong sub-millimetre (sub-mm) emission (Archibald et al. 2001; Reuland et al. 2004; Greve, Ivison & Stevens 2006), their mid-IR spectra (Seymour et al. 2008, Rawlings, in preparation) and the spectacular (>100 kpc) Lyα haloes sometimes observed (Reuland et al. 2003; Villar-Martín et al. 2003), showing the extended gas that can provide the fuel for star formation. To complement future targeted *Herschel* studies of the rare, very powerful radio-loud AGN, we examine in this work less luminous radio-loud AGN, $26.5 > \log(L_{1.4}/\mathrm{W\,Hz^{-1}}) \geq 25$, which can be found in reasonable abundance over areas of a few square degrees. We use this definition of 'radio-loud' AGN, based on radio luminosity density (e.g. Miller, Peacock & Mead 1990), in order to avoid making any distinction between type 1 and type 2 AGN, i.e. AGN classification based upon optical spectroscopy, where different amounts of AGN obscuration may affect the relative amount of optical emission. As we shall show, most of these sources are also 'radio-loud' when using the definition of Kellerman et al. (1989, 5 GHz over a *B*-band luminosity of >10). Star formation in these less luminous radio-loud AGN

remains poorly studied, as there has been no systematic follow-up of such sources above $z > 0.1$. Recently, the importance of radio-loud AGN in this luminosity range was demonstrated by Sajina et al. (2007) who found that 40 per cent of $z \sim 2$ ultraluminous infrared galaxies (ULIRGs) with deep silicate absorption features were radio-loud and these authors postulated that such sources are transition 'feedback' objects after the radio jet has turned on, but before feedback has halted black hole accretion and star formation.

The SPIRE instrument (Griffin et al. 2010) on board the *Herschel Space Observatory* (Pilbratt et al. 2010) gives us a clear view of the far-IR/sub-mm Universe at wavelengths where many galaxies emit most of their luminosity. The Herschel Multi-tiered Extragalactic Survey (HerMES;[1] Oliver et al., in preparation) provides deep IR SPIRE data over many of the best-studied extra-galactic survey fields. Recent results from *Herschel* show that SPIRE-detected AGN in deep HerMES fields have far-IR colours similar to the bulk of the SPIRE population which are believed to be star formation dominated (Elbaz et al. 2010; Hatziminaoglou et al. 2010), and modelling of their spectral energy distributions (SEDs) suggests that the SPIRE emission in AGN is dominated by a star-forming component (Hatziminaoglou et al. 2010).

The work presented here uses *Herschel*/SPIRE observations of the *Spitzer* Extragalactic First Look Survey (FLS) field taken as part of the *Herschel* Science Demonstration Phase (SDP) in 2009 October to November. Of the fields observed in SDP, this field had the best combination of wide area, uniform radio coverage and good multiwavelength follow-up. We present our sample of moderate- and high-redshift radio-loud AGN in Section 2 and derive IR luminosities and SFRs in Section 3. We present our results in Section 4 and discuss them in Section 5. We conclude this paper in Section 6. Throughout, we use a 'concordance' cosmology of $\Omega_{\rm M} = 1 - \Omega_\Lambda = 0.3$, $\Omega_0 = 1$ and $H_0 = 70\,{\rm km\,s^{-1}\,Mpc^{-1}}$.

2 SAMPLE

2.1 Radio sample and cross-identification

Our radio data come from the 1.4-GHz Very Large Array catalogue of Condon et al. (2003), which is complete down to 0.115 mJy (5σ). We restrict our analysis to a region of the FLS with complete optical and near-IR/mid-IR coverage, defined by $257.^\circ8 < {\rm RA} < 261^\circ$ and $58.^\circ6 < {\rm Dec.} < 60.^\circ4$. These optical to mid-IR ancillary data were taken from the Infrared Array Camera (IRAC) selected, multiwavelength data fusion catalogue in the FLS (hereafter, the FLS 'Data Fusion Catalogue') presented by Vaccari et al. (in preparation). The Data Fusion Catalogue is a *Spitzer*/IRAC-selected wide-area multiwavelength catalogue covering the ∼60-deg^2 extragalactic fields covered by *Spitzer*/IRAC and Multiband Imaging Photometer for *Spitzer* (MIPS) seven-band imaging. The main selection of the catalogue requires an IRAC 3.6- or 4.5-μm detection, since the two *Spitzer* channels reach about the same depth. MIPS 24-μm detections are associated with IRAC sources to improve their positional accuracy, and the MIPS 70- and 160-μm detections are confirmed by an MIPS 24-μm detection to increase their reliability.

In this paper, we use the version of the Data Fusion employed in HerMES SDP work. For the FLS field, we thus use the IRAC catalogue from Lacy et al. (2005), the MIPS 24-μm catalogue from Fadda et al. (2006), and MIPS 70- and 160-μm catalogues produced by the HerMES team using the SSC-provided software (e.g. Frayer et al. 2009). We combine the mid- and far-IR data from *Spitzer* with optical data (*ugriz*) from the Isaac Newton Telescope (Solares et al., in preparation) as well as redshift information from the literature.

Table 1. Composition of the FLS master radio catalogue. We indicate the total number of sources in the master catalogue, the number with cross-identifications in the FLS Data Fusion Catalogue and redshifts, and the number of sources with redshifts and SPIRE/250-μm detections.

Total number of radio sources	1907
With FLS Data Fusion XIDs and known redshifts	885
With SPIRE/250 μm and known redshifts	436

The redshifts come from the Sloan Digital Sky Survey (SDSS) spectroscopy and photometry as well as dedicated follow-up of many radio and mid-IR/far-IR selected targets by several groups (e.g. Martínez-Sansigre et al. 2005; Papovich et al. 2006; Weedman et al. 2006; Lacy et al. 2007; Marleau et al. 2007; Yan et al. 2007; Sajina et al. 2008; Dasyra et al. 2009). As the photometric redshifts from the SDSS do not extend accurately above $z = 1$, higher redshift sources will be dominated by the selection criteria of these different groups. We can compare the optical magnitudes and mid-IR flux densities of the sources with and without known redshifts. We find that around 100 radio sources with known redshifts are not detected in the z band, but are detected at 24 μm at brighter flux densities than most sources without redshift information. Hence, as faint z-band sources typically lie at higher redshifts, this observation is consistent with the specific targeting of bright 24-μm sources for spectroscopic follow-up at high redshift. We discuss how we deal with this selection in Section 4.

We cross-correlated the radio catalogue with the FLS Data Fusion Catalogue using a 2-arcsec search radius between the radio and mid-IR (3.6-μm) positions. Extended/multicomponent sources from Condon et al. (2003) were inspected by eye and five were reclassified as being two or more separate sources due to the presence of more than one optical/near-IR counterpart to individual radio components. We therefore obtained a master catalogue of 1907 radio sources of which 885 had spectroscopic or photometric redshifts from the Data Fusion Catalogue (see Table 1). We illustrate in Fig. 1 the distribution in redshift/luminosity space of the sources from the master catalogue with known redshifts. Our search radius and the sky density of the FLS Data Fusion Catalogue imply that 12/1571 (i.e. <1 per cent) of our cross-identifications are by chance.

While the redshift information for our sample is incomplete, it is only important for sources that potentially satisfy our radio luminosity selection criteria and are hence included in our radio-loud sample. However, in the subsequent sections we present the selection of our radio-loud AGN samples in two different redshift ranges, assess how complete these are by comparisons to models based on the known evolution of the high-redshift radio-loud population (see Section 2.3) and how this selection will effect our sample (see Section 4).

2.2 Radio-loud selection and sub-samples

To obtain accurate luminosities, radio spectral indices are required, so we cross-correlated the master catalogue with the 610-MHz catalogue of Garn et al. (2007) finding counterparts within 6 arcsec for 68 per cent of the master sample. We use a 6-arcsec search radius to account for the positional accuracy of the 610-MHz data. For radio sources without 610-MHz counterparts, we assumed a

[1] http://hermes.sussex.ac.uk

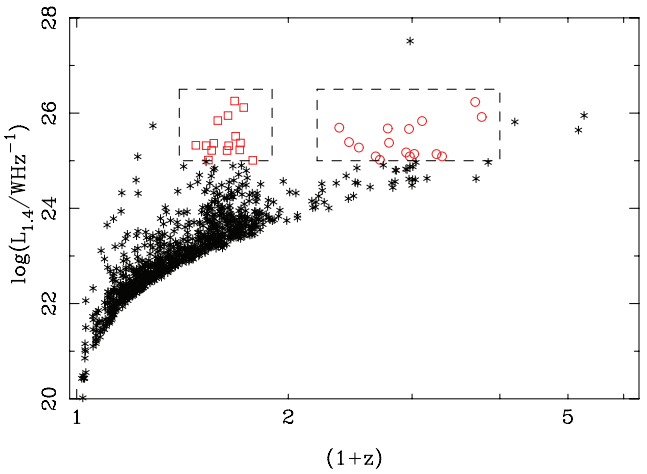

Figure 1. Redshift/radio luminosity distribution of 885/1907 radio sources in our master catalogue with known redshifts. The red symbols within the dashed rectangles indicate our moderate- and high-redshift sub-samples represented by squares and circles, respectively. Note that the sub-samples are chosen in redshift ranges where they are likely to be most complete (see Fig. 2).

spectral index with a value of $\alpha = -0.75$ ($S_\nu \propto \nu^\alpha$) consistent with the mean value found for faint radio sources in general (AGN and starbursts alike; e.g. Ibar et al. 2009). We note that the sample here has a slightly steeper mean radio spectral index ($\alpha = -0.82$), but the relative limits of the 1.4-GHz and 610-MHz survey result in bias against sources with a flat spectrum at low flux densities. We select our radio-loud AGN sample with luminosity density cuts of $25 \leq \log(L_{1.4}/\mathrm{W\,Hz^{-1}}) \leq 26.5$. The lower limit is chosen to ensure that our sources are genuinely radio-loud and to minimize the number of extreme star-forming galaxies (SFGs) selected. Indeed, this lower radio luminosity is equivalent to a total IR (8–1000 μm) luminosity of $\sim 3 \times 10^{13}\,\mathrm{L_\odot}$ from the correlation of far-IR and radio luminosities for SFGs (Yun & Carilli 2002) and therefore an SFR of $\sim 6000\,\mathrm{M_\odot\,yr^{-1}}$ using the relations of Kennicutt (1998). Hence, this luminosity would be extreme for a starburst galaxy. The upper limit is imposed as radio sources with luminosities greater than this cut are rare in the volume probed in this study. We find one source with such a luminosity ($L_{1.4} \sim 10^{27.5}\,\mathrm{W\,Hz^{-1}}$ at $z \sim 2$; see Fig. 1) which is identified as an SDSS quasi-stellar object (QSO). We consider it no further in this study, but note that this radio-loud QSO is not detected in our SPIRE observations. We also find that all our 'radio-loud' AGN would be classified as radio-loud by the rest-frame 5 GHz to *B*-band flux ratio according to the criteria of Kellerman et al. (1989) bar three sources in the high-redshift bin which have ratios just below the cut-off value of 10.

We then separate the luminous radio sources into moderate ($0.4 < z < 0.9$) and high ($1.2 < z < 3$) redshift samples with 15 and 16 sources, respectively [out of a total of 36 radio sources from the master catalogue with $25 < \log(L_{1.4}/\mathrm{W\,Hz^{-1}}) < 26.5$]. We chose these two redshift bins since the redshift distribution of the luminous radio sources peaks in these ranges (see Fig. 1), and hence we should obtain the most complete sub-samples possible given the data available (see below for estimates of their completeness). We note that the general decrease in known redshifts at $z \sim 1$ seen in Fig. 1 is due to the ineffectiveness of SDSS photometric and spectroscopic redshift estimation above this redshift. Hence, all the sources in the moderate-redshift sample have redshifts from SDSS (4/15 are spectroscopic with their remainder being photometric). Sources with higher known redshifts are generally from targeted follow-up of various classes of object as well as the occasional SDSS QSO. All the redshifts in the high-redshift bin are spectroscopic and come from these various follow-up projects. Interestingly, these two redshift ranges also cover similar length cosmic epochs of about 3 Gyr each. The median radio luminosities of both sub-samples are very similar: $\log(L_{1.4}/\mathrm{W\,Hz^{-1}}) = 24.9$ and 25.0 for the moderate- and high-redshift samples, respectively.

2.3 Completeness

In Fig. 2, we show the *observed* distribution of radio luminosities in each redshift sample and compare this to the *modelled* luminosity distributions over the same volume derived from the Square Kilometre Array (SKA) Simulated Skies (S-cubed; Wilman et al. 2008) at the radio flux density limit of the FLS (0.115 mJy). As well as the total number of sources predicted in these luminosity redshift bins, we also indicate the number of extreme SFGs (SFR $> 6000\,\mathrm{M_\odot\,yr^{-1}}$) predicted. The class of AGN from S-cubed which dominate this distribution is the low-luminosity radio-loud AGN (Wilman et al. 2008). The evolution of this population is taken from 'model C' of Willott et al. (2001) and is reasonably well constrained up to $z = 2$. We then apply a high-redshift decline in space density represented by $(1 + z)^{-2.5}$ above $z = 2.5$ as recommended in Wilman et al. (2008). There is also a small, ∼6 per cent, contribution to the number of sources predicted by S-cubed of 'radio-quiet' AGN whose evolution is less well constrained by observation. We have

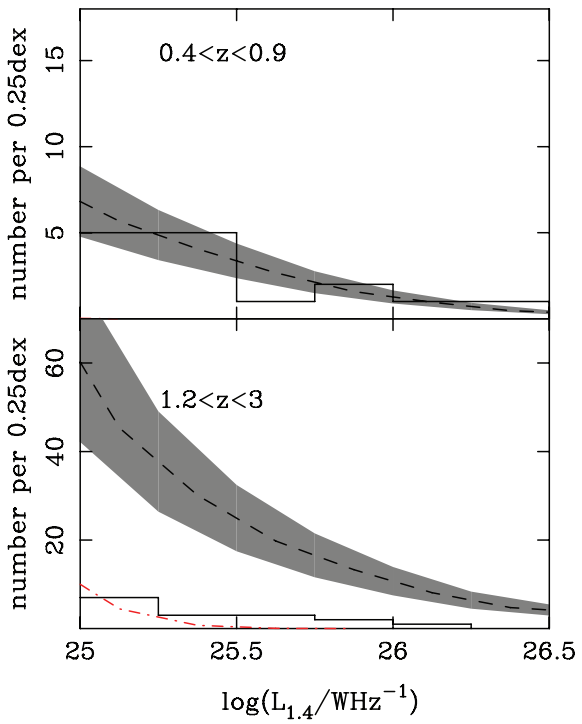

Figure 2. Observed number distribution versus radio luminosity density of sources in our moderate- and high-redshift samples (black solid histograms). The dashed line represents the distribution of the total number of radio sources expected in this volume from the SKA Simulated Skies (S-cubed; Wilman et al. 2008), where the number expected to be SFGs is indicated by the dot–dashed line (none is predicted in the moderate-redshift sample). The shaded region represents a 30 per cent uncertainty in S-cubed. In comparison to S-cubed, our moderate-redshift sample is 100 per cent complete and our high-redshift sample is 14 per cent complete.

Table 2. Composition of radio-loud AGN sub-samples. For both redshift sub-samples we present the number of sources predicted from S-cubed, the total number found, the number with SPIRE/250-μm detections, the mean 250-μm flux densities of the detected and undetected (via stacking techniques) sources, the mean SFR of the detected sources, the inferred mean SFR of the undetected sources (assuming that it scales directly with the mean 250-μm flux density), the total mean SFR of all observed sources and the range of mean SFRs given the number of sources predicted by S-cubed.

Description		Sub-sample	
		Moderate	High
S-cubed number predicted		16	116
Total number found		15	16
With SPIRE/250 μm $\sigma \geq 3$		4	9
$\langle S_{250}^{\rm detected} \rangle$	(mJy)	27.2 ± 2.5	39.2 ± 2.5
$\langle S_{250}^{\rm undetected} \rangle$	(mJy)	2.0 ± 0.8	6.5 ± 1.0
$\langle {\rm SFR}_{250}^{\rm detected} \rangle$	($M_\odot\,{\rm yr}^{-1}$)	92 ± 28	914 ± 274
$\langle {\rm SFR}_{250}^{\rm undetected} \rangle$	($M_\odot\,{\rm yr}^{-1}$)	6.7 ± 2.8	153 ± 23
$\langle {\rm SFR}_{250}^{\rm total} \rangle$	($M_\odot\,{\rm yr}^{-1}$)	29.5 ± 11.6	581 ± 143
Range of $\langle {\rm SFR} \rangle$	($M_\odot\,{\rm yr}^{-1}$)	18–41	80–581

included a 30 per cent uncertainty in the predicted number of radio sources from S-cubed to represent the uncertainty in the evolution of the luminosity function for the low-luminosity radio-loud AGN population, in particular the high-redshift cut-off and the less well constrained 'radio-quiet' population, as well as sample variance for a survey field covering only a few square degrees.

We find that our moderate-redshift sample is complete given the uncertainties we ascribed to S-cubed. However, we find that the number of sources predicted by S-cubed exceeds the number we observe in the high-redshift bin implying a 14 per cent completeness. The number of sources we find in each sub-sample compared to the number predicted from S-cubed is given in Table 2. The number of sources deficient in our high-redshift sample (and at other redshift ranges) can be accounted for by the lack of redshift information in the master sample (Table 1). We account for any bias in our samples, e.g. mid-IR selection of known high-redshift radio-loud AGN, in Section 4 by considering the full limits of the completeness and we demonstrate that we can still constrain the range of mean SFRs for these samples by making two extreme assumptions about the sources missing from our sample.

3 ANALYSIS

3.1 IR luminosities

We extracted SPIRE flux densities at the positions of all radio and 24-μm sources using the HerMES XID method (Roseboom et al. 2010). This approach minimizes the effect of source blending, as the SPIRE flux densities are estimated via linear inversion methods using the positions of known 24-μm sources, or radio position if there is no 24-μm counterpart, as a prior. In Roseboom et al. (2010), the 250-μm flux density uncertainty is estimated to be 7.45 mJy from injection and recovery of mock sources into the observed maps. Flux density uncertainties are obtained from the rms of input–output flux densities and consequently include contributions from both instrumental and confusion noise. We find 436 sources having 250-μm counterparts with $>3\sigma$ detections and known redshifts. For the

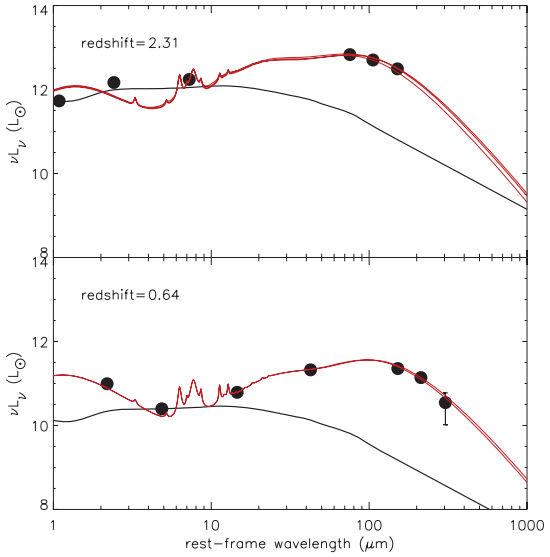

Figure 3. Example SED fits to the available IR photometry from 3.6 to 500 μm where we show rest-frame luminosity plotted against rest-frame wavelength. The red lines indicate the best-fitting starburst template and the range of templates within $\Delta\chi_i^2 < 1$ and the black lines indicate the maximum normalization of the AGN template to the lowest mid-IR photometry. The filled circles indicate the *Spitzer* and *Herschel* photometry used in the fitting. Note that in most cases, the uncertainties are smaller than the symbols. We present an object from both the low-redshift sample (lower panel, $z = 0.645$, $L_{\rm IR} = 5.77 \pm 0.58 \times 10^{11}\,{\rm L}_\odot$) and the high-redshift sample (upper panel, $z = 2.31$, $L_{\rm IR} = 1.84 \pm 0.17 \times 10^{13}\,{\rm L}_\odot$).

radio-loud sources we find 4/15 and 9/16 with significant 250-μm detections in the moderate- and high-redshift bins, respectively[2].

The relative depths of the 24- and 250-μm data available for this field have some bearing on how the 250-μm sources are found by the cross-identification (XID) method. The 24-μm imaging data of this field are relatively shallow with respect to the SPIRE data (compared to other fields to which this method has been applied). Hence, there may be non-negligible 250-μm flux remaining in the field which has not been extracted due to the lack of a 24-μm (or radio) counterpart. We visually inspected all 250-μm detections of the radio-loud sources in the SPIRE image and they all appear isolated with no sources close enough to them which could significantly effect the measurement of their SPIRE flux density.

We derive total (8–1000 μm) IR luminosities by fitting all the data available for the 436 radio sources across the *Spitzer*/IRAC+MIPS and *Herschel*/SPIRE bands following the method outlined in Symeonidis et al. (2009) (see Fig. 3). In all cases, we use the *Spitzer*/24-μm and *Herschel*/250-/350-/500-μm photometry although in some cases the 350- and 500-μm photometry have extremely large uncertainties due to their low signal-to-noise ratio (S/N), <3, and do not significantly affect the values of χ^2 derived. This fitting method uses all the models from Siebenmorgen & Krügel (2007), which cover a wide range of SED types, and finds the best fit using standard χ^2 minimization from which a total IR luminosity is calculated. Uncertainties in the IR luminosity are derived from the range of values obtained from SED fits which differ from the best fit by $\Delta\chi_i^2 = (\chi_i^2 - \chi_{\rm min}^2) < 1$.

[2] For reference, 24 per cent of the radio sources with unknown redshifts have significant detections in the SPIRE wavebands.

3.2 AGN contribution to the far-IR luminosity

A further issue to consider, if we are to use the total IR luminosities as indicators of SFR, is the AGN contribution to this luminosity which could lead to an overprediction of the SFRs. This issue is especially important because our sources are selected to be AGN. In a similar fashion to Symeonidis et al. (2010), we address this issue by normalizing a QSO template from Elvis et al. (1994) to the data point with the lowest luminosity from our photometric data set of 3.6–24 μm, as the AGN emission must be constrained by our photometry. If we use other AGN SED models [e.g. type 1 and type 2 AGN from Polletta et al. (2007)] we find that our estimates of the upper limits to the AGN luminosities and ratios of AGN to total IR luminosities change little, <10 per cent (and therefore even less for the final SFR). Such model SEDs are broadly similar to the Elvis et al. (1994) templates which in the IR are generally flat (in νL_ν) out to the far-IR where they then drop sharply. We note that only four of our high-redshift sources have mid-IR spectroscopy from Yan et al. (2007); hence, we do not use these data to constrain SED fits.

We then estimate the AGN contribution to the total IR luminosity by integrating the QSO template in the 8–1000 μm region and subtract this from our total IR luminosity to obtain a star-forming IR luminosity for each object. We can then convert this star-forming IR luminosity to an SFR using the Kennicutt (1998) relation. In Fig. 4, we show the AGN IR luminosity and the ratio of AGN to total IR luminosity as a function of radio luminosity density for the radio sources detected by SPIRE in our two redshift samples. The IR AGN luminosity has a large scatter which is largely due to the moderate-redshift sub-sample having lower IR AGN luminosities ($\sim 10^{11}$ $L_\odot$) than the high-redshift sub-sample ($\sim 10^{12}$ $L_\odot$), although we observe no trend with radio luminosity within a sub-sample.

We suspect that the greater AGN IR luminosities of the sources in the high-redshift sample are most likely due to a bias in the redshift identification towards sources with bright 24-μm flux densities

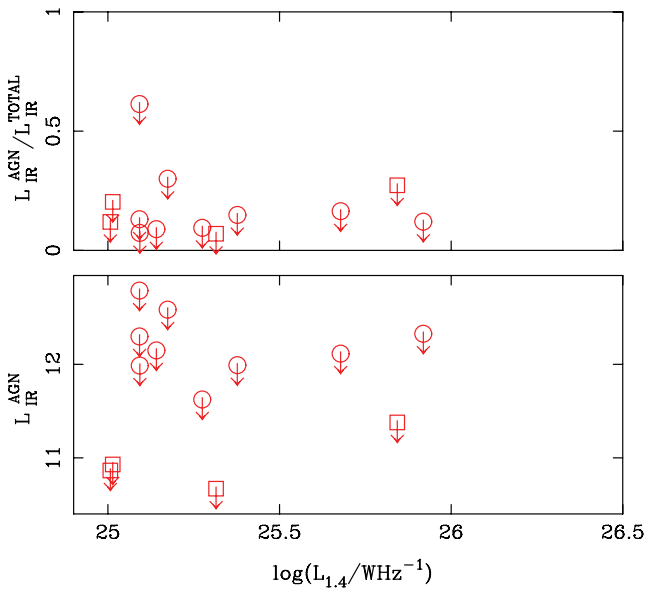

Figure 4. Upper limits to the AGN IR luminosity estimated from the normalization of an AGN SED to the lowest mid-IR luminosity, and the resulting upper limit to the ratio of AGN to total IR luminosity, both plotted as a function of radio luminosity density. These sources are from both our moderate- and our high-redshift samples (open squares and circles, respectively).

(≥1 mJy) as discussed in Section 2.1. Additionally, the flux-limited nature of the *Spitzer* and *Herschel* data means that the SPIRE observations are more sensitive to lower IR luminosities at lower redshifts. As these identified sources comprise just 14 per cent of the high-redshift sample, they are not likely to be representative in terms of their AGN fraction.

The ratio of AGN to total IR luminosity tends to be low, under 0.3 bar one source, consistent with the results seen in Hatziminaoglou et al. (2010), and averages around 0.15. As a check, we apply the simultaneous AGN/starburst template fitting routine used by Hatziminaoglou et al. (2010) to the radio-loud AGN studied here and we find similar total IR luminosities and AGN fractions. Therefore, the final SFRs we derive are not very sensitive to our choice of model starburst and AGN SEDs. Our assumption that the mid-IR is completely dominated by the AGN, while conservative, also does not have a strong effect on the final SFR due to the low AGN fraction.

3.3 Comparison between radio and IR luminosities

We calculate the total IR luminosities of all SPIRE-detected sources in order to confirm our method of measuring these luminosities by comparison with the radio/far-IR correlation seen in local SFGs and now confirmed at higher redshifts (Seymour et al. 2009; Ivison et al. 2010). Additionally, by extrapolating this empirical correlation to higher luminosities we can assess the contribution of star formation to brighter radio sources. Our radio luminosity selection would be equivalent to an SFR of $\sim$6000 $M_\odot$ yr^{-1} for a pure SFG, but potentially there could be a few sources with higher SFRs within the volume probed here (see S-cubed predictions in Fig. 2).

We find a strong correlation between the radio and IR luminosities, particularly below $L_{1.4} = 10^{24}$ W Hz^{-1} and $L_{\rm IR} = 10^{12.5}$ $L_\odot$ (see Fig. 5) which we use to verify our IR luminosities. Note that the IR luminosities of the radio sources in the moderate- and high-redshift samples have had the AGN contribution removed. We define the ratio of radio to IR luminosity as $q_{\rm IR} = \log(L_{\rm IR}/L_{1.4}) + 14.03$ [as used in Sajina et al. (2008), this definition is an equivalent but a more convenient form than the classical one of Helou, Soifer & Rowan-Robinson (1985)]. By fitting the correlation over these luminosity ranges we get a value of $q_{\rm IR} = 2.40 \pm 0.19$ using a biweight estimator (Beers, Flynn & Gebhardt 1990), in good agreement with the value found locally (Yun & Carilli 2002) and at higher redshift (Ivison et al. 2010).

We then assume that this relation holds to higher luminosities (i.e. to SFRs of >6000 $M_\odot$ yr^{-1}) and note that two radio sources with $\log(L_{1.4}/{\rm W\,Hz^{-1}}) > 25$ lie just within 2σ of $q_{\rm IR}$ The proximity of these two sources to the correlation may mean that these sources have a non-negligible contribution of star formation to their radio luminosity. The AGN fraction of the total IR luminosities for these sources is low, ≤10 per cent. However, upon closer inspection these two sources have radio spectra which are either too steep, $\alpha_{1.4}^{610} = -1.78$, or too flat, $\alpha_{1.4}^{610} = -0.22$, compared to the canonical value for SFGs (Condon 1992). The fraction of the radio luminosity due to star formation, assuming that the star-forming component lies precisely on the correlation, is 25–30 per cent. Hence, we conclude that their radio emission is dominated by AGN processes and retain them within our high-redshift sample.

3.4 Stacking the non-detections at 250 μm

We can obtain an approximate constraint on the far-IR luminosity of the radio-loud AGN not detected at 250 μm in each sample

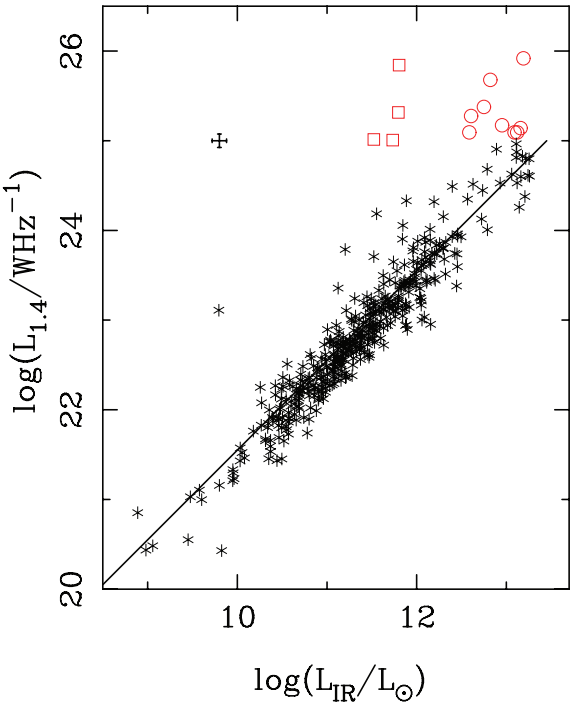

Figure 5. Total IR luminosity plotted against radio luminosity for all the FLS radio sources with redshifts and a $>3\sigma$ detection at 250 μm (including confusion noise). The sample of luminous radio sources, $L_{1.4} > 10^{25}\,\mathrm{W\,Hz^{-1}}$, used in this work is indicated by open symbols and the less luminous radio sources by asterisks. Note that the IR luminosities of the luminous radio sources do not include the AGN contribution (see Section 3.3). We fit the observed correlation in luminosities for $L_{1.4\,\mathrm{GHz}} < 10^{24}\,\mathrm{W\,Hz^{-1}}$ and $L_{\mathrm{IR}} < 10^{12.5}\,\mathrm{L_\odot}$ and derive $q_{\mathrm{IR}} = 2.40 \pm 0.19$. Two radio-loud AGN lie above, but within 2σ of this correlation; however, they have radio spectral indices inconsistent with star formation. Hence, we conclude that their radio emission is dominated by AGN processes.

by employing stacking techniques to obtain mean 250-μm flux densities for these sources. By assuming the same distribution of redshifts, IR SED types and ratios of AGN to total IR luminosity, we can argue that the mean SFRs of the undetected and detected samples scale directly with the 250-μm flux densities within both redshift ranges. Therefore, we stacked the 11 and seven sources not detected at 250 μm in each sub-sample and found the mean flux densities reported in Table 2. The uncertainties in flux densities of the stacked sources are simply those of the mean.

3.5 SFRs in local ($z < 0.1$) radio-loud AGN

In order to examine any evolution of the mean SFR of radio-loud AGN over cosmic time, we need a local baseline to compare with. Recently published *Spitzer*/MIPS observations of the local ($z < 0.1$) 3CRR sample (Dicken et al. 2010) provide an excellent opportunity to assess star formation in the nearby radio-loud population. The 1.4-GHz luminosity densities of this sample, derived from the 5-GHz values in Dicken et al. (2010) assuming $\alpha = -0.75$ and $S_\nu \propto \nu^\alpha$, fall within the $25 < \log(L_{1.4}/\mathrm{W\,Hz^{-1}}) < 26.5$ range of our sub-sample selection. The 3CRR sources were selected to only include sources with Fanaroff–Riley Class II (FRII) morphologies (i.e. those with radio lobes which are brightest at their edges; Fanaroff & Riley 1974). However, the lower radio luminosity density limit used in our work very closely corresponds to the luminosity density, $\log(L_{1.4}/\mathrm{W\,Hz^{-1}}) = 25.1$, at which the radio-loud population switches from mostly containing Class I sources to mostly containing Class II sources. Furthermore, this local sample is not sensitive to the low end of our radio luminosity density range at $z = 1$ and therefore may not be 100 per cent complete. Dicken et al. (2010) derived rest-frame 70-μm luminosities from their *Spitzer*/MIPS observations which they compare with the [O III] emission-line luminosities of the local 3CRR sample. They found a broad correlation implying that generally the 70-μm luminosity is due to the AGN. However some 3CRR sources, which show evidence of star formation from their optical spectra, generally lie above this correlation, i.e. they have an excess of 70-μm luminosity compared to the [O III] emission. These authors postulate that this 70-μm excess could be due to star formation.

Here, we estimate the range of mean SFR in this sample using two assumptions. To obtain an upper limit, we assume that *all* of the 70-μm luminosity is due to star formation. To obtain a lower limit, we use the linear regression fit by Dicken et al. (2010) to the correlation of the O III and 70-μm luminosities to estimate the AGN-only 70-μm luminosity. We then subtract the AGN luminosity from the total 70-μm luminosity for all sources lying more than 0.3 dex above the correlation in order to obtain a starburst-only 70-μm luminosity. In both cases, we convert the 70-μm luminosities to total IR luminosities using the relation of Symeonidis et al. (2008) and then to SFRs using the Kennicutt (1998) relation as before. Due to the size of the sample and the influence of one very luminous source, we use the median-inferred SFR and find that the range of typical SFRs for the local 3CRR sample is 3.4–4.2 $\mathrm{M_\odot\,yr^{-1}}$ from these two assumptions.

4 RESULTS

In Table 2 we report the mean SFR, ⟨SFR⟩, of the radio-loud AGN detected at 250 μm in each sub-sample. The SFRs of individual sources are derived from the total IR luminosities, minus the AGN contribution (see Section 3.2), using the conversion factors of Kennicutt (1998). We find values of 92 ± 28 and $914 \pm 274\,\mathrm{M_\odot\,yr^{-1}}$ in the moderate- and high-redshift bins, respectively. For the sources undetected at 250 μm, we find stacked 250-μm flux densities which are a factor of 11 and 7 lower than the mean flux densities of the detected sources (see Table 2) for the moderate- and high-redshift sub-samples, respectively. It is unsurprising that undetected sources have a mean flux density lower than those detected, but the fact that they are considerably lower (i.e. not just below our 3σ cut) suggests that these radio-loud AGN have a wide range of intrinsic SFRs. We report the SFRs of the undetected sources in Table 2 obtained from the ratio of the mean 250-μm flux densities of the detected and undetected sources and the measured SFR of the detected sources. Then we estimate the total mean SFR in each subset by combining the mean SFR of the detected and undetected sources weighted by the number in each group. The estimated total mean SFRs for the total sample are therefore 29.5 ± 11.6 and $581 \pm 143\,\mathrm{M_\odot\,yr^{-1}}$ for the moderate- and high-redshift bins, respectively.

The moderate-redshift sample is complete within the uncertainties of the S-cubed simulation (we find 15/16 predicted sources in this redshift/luminosity density parameter space). Hence, we can directly calculate the mean SFR of the low-redshift sample by summing the observed SFRs and dividing by the number sources. The uncertainties are simply those of the measured SFRs, which directly come from the uncertainties in the IR luminosities, combined with the 30 per cent uncertainty in the S-cubed model. As the latter are so much greater than the former, our uncertainties are dominated by the conservative uncertainties we used in S-cubed. We find a

mean SFR for this sub-sample of $29.5 \pm 11.6\,M_\odot\,yr^{-1}$ which is equivalent to the range of values of 18–41 $M_\odot\,yr^{-1}$.

As we saw from Fig. 2 the high-redshift sub-sample is incomplete, although we can quantify the incompleteness from comparisons to the S-cubed simulation. The number of radio-loud AGN expected from S-cubed is given in Table 2. We cannot estimate the properties of sources not included in our high-redshift sample due to lack of redshift information. However, we can estimate likely lower and upper limits on the mean SFR from two simple assumptions. First, to estimate the lower limit we assume that all the sources missed have SFRs of zero and then scale the mean SFR by the incompleteness (i.e. the lower limit is $\frac{16}{116}\times$ the mean SFR for the observed fraction). While 24 per cent of the sources with unknown redshifts have 250-μm detections, we have no way of knowing how many of these fall into our high-redshift sub-sample; hence, this method of determining our lower limit is the most robust approach. Secondly, for the upper limit we assume that all sources not included have mean SFRs identical to the detected fraction, i.e. the upper limit is simply the measured mean SFR for the detected fraction. Hence, we calculate the range of mean SFRs for the high-redshift sub-sample to be 80–581 $M_\odot\,yr^{-1}$.

We compare these constraints with those found for the local 3CRR sample and the recent results of Hardcastle et al. (2010) in Fig. 6 who measured IR luminosities from *Herschel*-ATLAS observations of radio sources occupying a similar region of redshift/luminosity parameter space. We see an increase in the mean SFR of radio-loud AGN with cosmic look-back time. In the local Universe we found the mean SFR of $z < 0.1$ radio-loud AGN to be 3.4–4.2 $M_\odot\,yr^{-1}$, whereas at moderate redshifts, $0.4 < z < 0.9$, we constrain it to be approximately five to 10 times greater and in our high-redshift sample we find it to be ∼20–150 times greater. While these ranges of mean SFRs are wide, we observe a clear trend of increasing mean SFR with redshift in radio-loud AGN in the luminosity density range $25 < \log(L_{1.4}/W\,Hz^{-1}) < 26.5$, a trend that is also seen over a smaller redshift range in the results of Hardcastle et al. (2010).

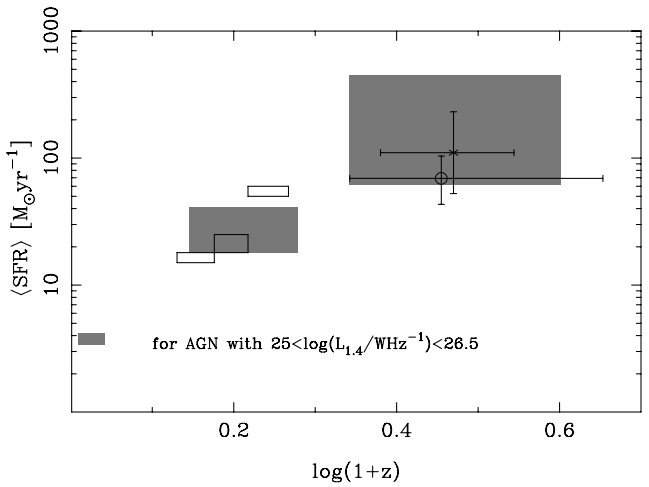

Figure 6. Range of mean SFRs plotted as a function of redshift for radio-loud AGN with $25 \leq \log(L_{1.4}/W\,Hz^{-1}) \leq 26.5$ (shaded regions). At $0 < z < 0.1$ the data are from our 3CRR local reference sample and at $0.4 < z < 0.9$, and $1.2 < z < 3.0$ from our moderate- and high-redshift sub-samples respectively. The open rectangles indicate the results from Hardcastle et al., (2010) using *Herschel* observations of sources with a similar range of radio luminosities. The points with error bars present the approximate mean SFRs of X-ray-selected AGN over the range of redshifts indicated from Lutz et al. (2010, open circle) and Shao et al. (2010, asterisk).

We can quantify this rate of increase by fitting a straight line through the shaded regions of Fig. 6 via linear regression. We then find that the mean SFR of radio-loud AGN in this luminosity range evolves as $(1+z)^Q$, where we measure the value of $Q = 4.2 \pm 0.8$. This value for the evolution is strong and greater than that measured for the evolution of the star-forming luminosity function (which typically has values of $Q \sim 3$ as traced by IR surveys; Le Floc'h et al. 2005; Huynh et al. 2007; Magnelli et al. 2009; Rodighiero et al. 2010). We can also compare our results with the mean SFRs of high-redshift AGN selected at other wavelengths. The mean SFRs of X-ray-selected AGN, $L_{2\text{-}10\,keV} > 10^{43}\,erg\,s^{-1}$, have been recently studied by Shao et al. (2010) and Lutz et al. (2010) who found that such sources have mean SFRs within, but at the low end of, the range of values found in our high-redshift bin. We illustrate these results in Fig. 6 using the same Kennicutt total IR luminosity to SFR conversion as before and converting the Shao et al. 60-μm monochromatic luminosities using the formula presented in Symeonidis et al. (2008). Also, Hatziminaoglou et al. (2010) found a similar range of SFRs for a heterogeneous sample of AGN above $z = 1$, suggesting that this increase is common to different types of AGN activity.

If we sum the observed star formation in each redshift bin, we can calculate the comoving SFR density due to the host galaxies of the radio-loud AGN in each redshift sub-sample. We find values of $\sim 2.5 \times 10^{-5}\,M_\odot\,yr^{-1}\,Mpc^{-3}$ for the moderate-redshift bin and $1\text{–}5 \times 10^{-4}\,M_\odot\,yr^{-1}\,Mpc^{-3}$ for the high-redshift bin. For the local redshift bin, the star formation density due to the host galaxies of the radio-loud AGN is $\sim 4 \times 10^{-8}\,M_\odot\,yr^{-1}\,Mpc^{-3}$. We can compare these SFR densities with the globally measured SFR history from a variety of different methods (e.g. Hopkins & Beacom 2006). We observe that the relative contribution of the host galaxies of radio-loud AGN to the total comoving SFR density increases with redshift from ∼0.0004 per cent in the local sample to ∼0.03 and ∼0.1–0.5 per cent for the moderate- and high-redshift samples, respectively.

In Fig. 7, we show the ⟨SFR⟩ as a function of radio luminosity density for each of our two redshift sub-samples. We calculate upper and lower limits for each luminosity density bin as we did for the whole sample. The upper and lower limits are indicated by the grey-shaded regions. Note that due to the fact that we only detect 4/15 sources in the moderate-redshift sample, we have to increase the bin size by a factor of 3 compared to the high-redshift sample. We also overlay the upper and lower limits for the whole of each sub-sample as indicated by the dashed lines. We see no evidence for any trend of mean SFR with radio luminosity for either sub-sample, although the constraints for the highest radio luminosity density bin of the high-redshift sample are not so strong.

5 DISCUSSION

We observe that radio-loud AGN in the distant Universe have an increasing mean SFR with cosmological look-back time in the $25 < \log(L_{1.4}/W\,Hz^{-1}) < 26.5$ radio luminosity density range. In the local Universe, $z < 0.1$, the mean SFR of the 3CRR sample is five to 10 times less than that in a moderate-redshift sample, $0.4 < z < 0.9$. We note that the 3CRR sample was also selected on FRII radio morphology which suggests that we may not be comparing identical populations, and it may not be 100 per cent complete. Another recent study has examined the IR luminosities of bright radio sources with *Herschel*-ATLAS observations of the GAMA-9h field.

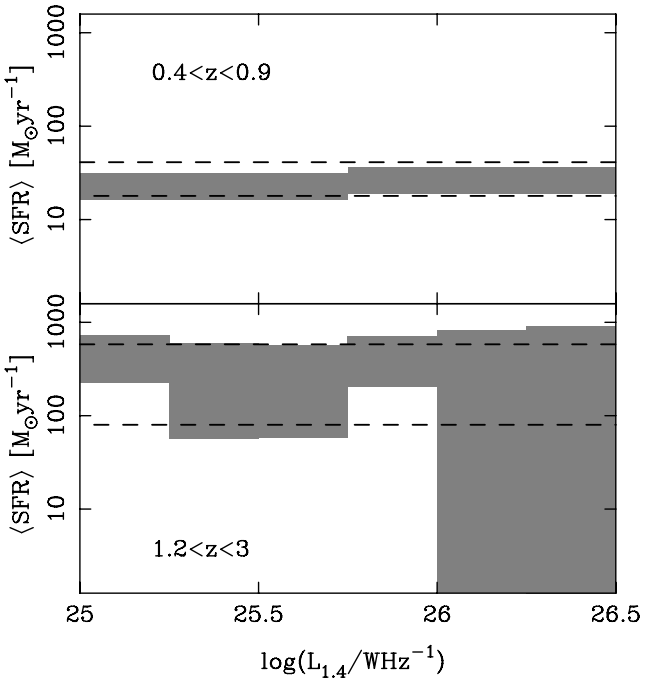

Figure 7. Mean star formation rate, ⟨SFR⟩, of the host galaxies of radio-loud AGN plotted as a function of radio luminosity density for each of the redshift sub-samples. The shaded regions for each bin then represent the range of ⟨SFR⟩ assuming either (i) all the sources missed have ⟨SFR⟩ = 0 (the lower limit) or (ii) all the sources missed have ⟨SFR⟩ equal to the sources found. The dashed lines represent the range of ⟨SFR⟩ for the whole of each redshift sample as given in Table 2.

With a similar radio luminosity cut to our moderate-redshift sub-sample, Hardcastle et al. (2010) found a mean SFR of between 20 and 50 $M_\odot$ yr^{-1}, increasing across our moderate-redshift bin (see Fig. 6). This range of mean SFRs is consistent with that found here, 18–41 $M_\odot$ yr^{-1}, allowing for the slightly different source selection, the different method of estimating IR luminosities and the fact that these authors do not subtract any AGN contribution from the total IR luminosity.

We find the increase in the mean SFR of radio-loud AGN hosts [parametrized as $\sim(1+z)^Q$, $Q = 4.2 \pm 0.8$] to be greater than that of the IR luminosity function which traces the evolution of the general star-forming population. This greater rate of increase with redshift, compared to the regular star-forming population, suggests that some of the star formation may be directly associated with the radio-loud AGN activity. The increase in mean SFR with redshift of AGN is also seen in X-ray-selected AGN (e.g. Lutz et al. 2010; Shao et al. 2010) and in a heterogeneous sample of AGN (Hatziminaoglou et al. 2010). Alternatively, our results could reflect an increase in the stellar mass of the host galaxy, since high stellar mass galaxies have SFRs which increase with redshift (e.g. Juneau et al. 2005). This interpretation would fit in with the recent Tadhunter et al. (2011) result who found that at low redshifts, $z < 0.7$, not all ULIRGs are massive enough to host radio-loud AGN. If the stellar masses of ULIRGs increase with redshift, then ULIRGs would be more likely to host radio-loud AGN at higher redshifts.

While it is likely that the redshift information for the high-redshift sample is biased towards sources that have bright 24-μm flux densities (see Section 2.1), our approach of determining a range of mean SFRs given two extreme assumptions alleviates much of the concern about selection bias. The remaining principle source of uncertainty is the S-cubed model, used to quantify how complete our sub-samples were. As discussed earlier, our uncertainties in S-cubed are very conservative. S-cubed treats the AGN and SFGs as separate populations, i.e. it does not include hybrid radio sources exhibiting both processes simultaneously. We can thereby compare the expected number of radio-loud AGN regardless of whether there is ongoing star formation in their hosts or not. The contribution to the SFR density of the host galaxies of radio-loud AGN in the high-redshift bin is interesting as the SFR density at this epoch is dominated by LIRGs and ULIRGs (Le Floc'h et al. 2005; Seymour et al. 2010). As 0.1–0.5 per cent of the SFR density consists of LIRGs and ULIRGs which host the radio-loud AGN, we can infer a duty cycle of 0.001–0.005 for radio-loud AGN activity in such sources, assuming that each LIRG and ULIRG goes through at least one radio-loud phase. The typical time-scale of a radio-loud phase of an AGN is around ∼10 Myr for extended radio sources (Miley 1980) and likely shorter for the less luminous sources with smaller radio lobes considered here. Given this lifetime and the estimated duty cycle of 0.001–0.005, we can estimate that LIRGs and ULIRGs undergo a radio-loud AGN phase every 2–10 Gyr. Hence, during the 3-Gyr time-span covered by the high-redshift sub-sample, we could expect perhaps one major phase of radio-loud AGN activity at a rate similar to that expected from major mergers (Hopkins et al. 2010).

The feedback models which quench star formation by evoking a radio-loud phase (e.g. Bower et al. 2006; Croton et al. 2006) are most important at late times, i.e. below $z < 1$, but they must occur at higher redshifts in order to prevent the most massive galaxies, formed at early times, from growing significantly more. However, in this work we observe many AGN in our high-redshift sub-sample which are in a state equivalent to the 'radio-mode' feedback of Croton et al. (2006) and Bower et al. (2006) and simultaneously have very high SFRs while feedback processes are predicted to be occurring.

6 CONCLUSIONS

We have examined the incidence of far-IR emission and inferred SFR of luminous radio-loud AGN in a moderate-redshift, $0.4 < z < 0.9$, and a high-redshift sub-sample, $1.2 < z < 3$, as well as in a local, $z < 0.1$, comparison sample. We have

(i) constrained the mean SFR of radio-loud AGN to be 3.4–4.2, 18–41 and 80–581 $M_\odot$ yr^{-1} for the local, moderate- and high-redshift samples, respectively; hence, we measure the evolution of the mean SFR to be $\sim(1+z)^{4.2\pm0.8}$;

(ii) observed no strong trends of SFR with radio luminosity in any redshift bin;

(iii) estimated that the host galaxies of radio-loud AGN in the high-redshift sub-sample contribute 0.1–0.5 per cent to the total SFR density at that epoch and if all LIRGs and ULIRGs have a radio-loud phase, we infer a duty cycle of 0.001–0.005 in such sources.

These results demonstrate that in the distant Universe a considerable amount of star formation is occurring in galaxies hosting a radio-loud AGN, consistent with the frequent evidence for high SFRs in classic high-redshift radio galaxies. The mean SFR evolves more quickly than the IR luminosity function implying that some of the star formation is directly related to the radio-loud AGN activity. Both starburst and active nuclear processes have relatively short time-scales, so their co-existence in many objects suggests that bursts of star formation and jet activity are either quite common or connected via 'feedback'. But is the jet initiating or quenching star formation, or are the processes independent? We cannot answer

such questions here, but we shall be able to do so with follow-up of individual sources (to search for outflows of jet-triggered star formation or for mergers triggering both) and with the huge sample that will be provided by the full HerMES data set combined with improved redshift information.

ACKNOWLEDGMENTS

NS thanks Carlos De Breuck, Martin Hardcastle, Curtis Saxton and Clive Tadhunter for useful discussions. SPIRE has been developed by a consortium of institutes led by Cardiff Univ. (UK) and including Univ. Lethbridge (Canada); NAOC (China); CEA, LAM (France); IFSI, Univ. Padua (Italy); IAC (Spain); Stockholm Observatory (Sweden); Imperial College London, RAL, UCL-MSSL, UKATC, Univ. Sussex (UK) and Caltech, JPL, NHSC, Univ. Colorado (USA). This development has been supported by national funding agencies: CSA (Canada); NAOC (China); CEA, CNES, CNRS (France); ASI (Italy); MCINN (Spain); SNSB (Sweden); STFC (UK) and NASA (USA). The data presented in this paper will be released through the Herschel Database in Marseille HeDaM (hedam.oamp.fr/HerMES).

REFERENCES

Aird J. et al., 2010, MNRAS, 401, 2531
Archibald E. N., Dunlop J. S., Hughes D. H., Rawlings S., Eales S. A., Ivison R. J., 2001, MNRAS, 323, 417
Beers T. C., Flynn K., Gebhardt K., 1990, AJ, 100, 32
Borys C., Smail I., Chapman S. C., Blain A. W., Alexander D. M., Ivison R. J., 2005, ApJ, 635, 853
Bower R. G. et al., 2006, MNRAS, 370, 645
Casey C. M. et al., 2009, MNRAS, 399, 121
Condon J. J., 1992, ARA&A, 30, 575
Condon J. J., Yin Q. F., Thuan T. X., Boller T., 1998, AJ, 116, 2682
Condon J. J., Cotton W. D., Yin Q. F., Shupe D. L., Storrie-Lombardi L. J., Helou G., Soifer B. T., Werner M. W., 2003, AJ, 125, 2411
Croft S. et al., 2006, ApJ, 647, 1040
Croton D. J. et al., 2006, MNRAS, 365, 11
Dasyra K. M. et al., 2009, ApJ, 701, 1123
Dicken D., Tadhunter C., Axon D., Robinson A., Morganti R., Kharb P., 2010, ApJ, 722, 1333
Elbaz D. et al., 2010, A&A, 518, L29
Elvis M. et al., 1994, ApJS, 95, 1
Fadda D. et al., 2006, AJ, 131, 2859
Fanaroff B. L., Riley J. M., 1974, MNRAS, 167, 31
Fragile P. C., Murray S. D., Anninos P., van Breugel W., 2004, ApJ, 604, 74
Frayer D. T. et al., 2009, AJ, 138, 1261
Garn T., Green D. A., Hales S. E. G., Riley J. M., Alexander P., 2007, MNRAS, 376, 1251
Giavalisco M. et al., 2004, ApJ, 600, L103
Greve T. R., Ivison R. J., Stevens J. A., 2006, Astron. Notes, 327, 208
Griffin M. J. et al., 2010, A&A, 518, L3
Hardcastle M. J. et al., 2010, MNRAS, 409, 122
Hatziminaoglou E. et al., 2008, MNRAS, 386, 1252
Hatziminaoglou E. et al., 2010, A&A, 518, L33
Helou G., Soifer B. T., Rowan-Robinson M., 1985, ApJ, 298, L7
Hopkins A. M., Beacom J. F., 2006, ApJ, 651, 142
Hopkins P. F. et al., 2010, ApJ, 724, 915
Huynh M. T., Frayer D. T., Mobasher B., Dickinson M., Chary R., Morrison G., 2007, ApJ, 667, L9
Ibar E., Ivison R. J., Biggs A. D., Lal D. V., Best P. N., Green D. A., 2009, MNRAS, 397, 281
Ivison R. J. et al., 2010, A&A, 518, L31
Juneau S. et al., 2005, ApJ, 619, L135
Kellerman K. I., Sramek R., Schmidt M., Shaffer D. B., Green R., 1989, AJ, 98, 1195
Kennicutt R. C., 1998, ARA&A, 36, 189
Lacy M. et al., 2005, ApJS, 161, 41
Lacy M. et al., 2007, AJ, 133, 186
Le Floc'h E. et al., 2005, ApJ, 632, 169
Lutz D. et al., 2010, ApJ, 712, 1287
Magnelli B., Elbaz D., Chary R. R., Dickinson M., Le Borgne D., Frayer D. T., Willmer C. N. A., 2009, A&A, 496, 57
Magorrian J. et al., 1998, AJ, 115, 2285
Marleau F. R., Fadda D., Appleton P. N., Noriega-Crespo A., Im M., Clancy D., 2007, ApJ, 663, 218
Martínez-Sansigre A., Rawlings S., Lacy M., Fadda D., Marleau F. R., Simpson C., Willott C. J., Jarvis M. J., 2005, Nat, 436, 666
Mauch T., Sadler E. M., 2007, MNRAS, 375, 931
Miley G., 1980, ARA&A, 18, 165
Miley G., De Breuck C., 2008, A&AR, 15, 67
Miller L., Peacock J. A., Mead A. R. G., 1990, MNRAS, 244, 207
Nesvadba N. P. H., Lehnert M. D., Eisenhauer F., Gilbert A., Tecza M., Abuter R., 2006, ApJ, 650, 693
Nesvadba N. P. H., Lehnert M. D., De Breuck C., Gilbert A. M., van Breugel W., 2008, A&A, 491, 407
Papovich C. et al., 2006, AJ, 132, 231
Pilbratt G. L. et al., 2010, A&A, 518, L1
Polletta M. et al., 2007, ApJ, 663, 81
Reuland M. et al., 2003, ApJ, 592, 755
Reuland M., Röttgering H., van Breugel W., De Breuck C., 2004, MNRAS, 353, 377
Rodighiero G. et al., 2010, A&A, 515, A8
Roseboom I. G. et al., 2010, MNRAS, 409, 48
Sajina A., Yan L., Lacy M., Huynh M., 2007, ApJ, 667, L17
Sajina A. et al., 2008, ApJ, 683, 659
Saxton C. J., Bicknell G. V., Sutherland R. S., Midgley S., 2005, MNRAS, 359, 781
Seymour N. et al., 2007, ApJS, 171, 353
Seymour N. et al., 2008, ApJ, 681, L1
Seymour N., Huynh M., Dwelly T., Symeonidis M., Hopkins A., McHardy I. M., Page M. J., Rieke G., 2009, MNRAS, 398, 1573
Seymour N., Symeonidis M., Page M. J., Huynh M., Dwelly T., McHardy I. M., Rieke G., 2010, MNRAS, 402, 2666
Shao L. et al., 2010, A&A, 518, L26
Siebenmorgen R., Krügel E., 2007, A&A, 461, 445
Springel V. et al., 2005, Nat, 435, 629
Symeonidis M., Willner S. P., Rigopoulou D., Huang J.-S., Fazio G. G., Jarvis M. J., 2008, MNRAS, 385, 1015
Symeonidis M., Page M. J., Seymour N., Dwelly T., Coppin K., McHardy I., Rieke G. H., Huynh M., 2009, MNRAS, 397, 1728
Symeonidis M., Rosario D., Georgakakis A., Harker J., Laird E. S., Page M. J., Willmer C. N. A., 2010, MNRAS, 403, 1474
Tadhunter C. et al., 2011, MNRAS, doi:10.1111/j.1365-2966.2010.17958.x
van Breugel W., Filippenko A. V., Heckman T., Miley G., 1985, ApJ, 293, 83
Villar-Martín M. et al., 2003, MNRAS, 346, 273
Wall J. V., Jackson C. A., Shaver P. A., Hook I. M., Kellermann K. I., 2005, A&A, 434, 133
Weedman D. W., Le Floc'h E., Higdon S. J. U., Higdon J. L., Houck J. R., 2006, ApJ, 638, 613
Willott C. J., Rawlings S., Blundell K. M., Lacy M., Eales S. A., 2001, MNRAS, 322, 536
Wilman R. J. et al., 2008, MNRAS, 388, 1335
Yan L. et al., 2007, ApJ, 658, 778
Yun M. S., Carilli C. L., 2002, ApJ, 568, 88

This paper has been typeset from a TEX/LATEX file prepared by the author.